Bootstrap Method for Uncertainty Evaluation in Critical Dimension Small-Angle X-Ray Scattering

Tianjuan Yang, Xiuguo Chen, Shuo Liu, Jiahao Zhang, and Shiyuan Liu

***Abstract*— Uncertainty evaluation is essential in critical dimension small-angle X-ray scattering (CD-SAXS) as it reflects the reliability of the measurement results. In this work, we introduce a new version of the bootstrap method for uncertainty evaluation in CD-SAXS to obtain both mean values and their associated uncertainties of nanostructure parameters. We further incorporate a more suitable centered bootstrap percentile method and a bias correction procedure for skewed bootstrap distributions in CD-SAXS. Subsequently, we conduct simulations and measurements on CD-SAXS using both 1-D and 2-D gratings. The accuracy of the proposed method is verified by comparison with the optical critical dimension (OCD), and the precision of the proposed method is verified by comparison with the Markov chain Monte Carlo (MCMC) method. The results indicate that the proposed bootstrap method is an effective candidate for uncertainty evaluation in CD-SAXS and other model-based measurement techniques.**

***Index Terms*— Bootstrap method, critical dimension small-angle X-ray scattering (CD-SAXS), inverse problem, nanostructure reconstruction, uncertainty evaluation.**

I. Introduction

CRITICAL dimension (CD) metrology plays a pivotal role in ensuring precise process control within the realm of integrated circuit (IC) manufacturing [1], [2], [3]. CD small-angle X-ray scattering (CD-SAXS) emerges as promising metrology for in-line measurement of future technology nodes, particularly in monitoring high-aspect-ratio and buried features. It is essentially a model-based measurement technique that uses subnanometer wavelength radiation in transmission mode [4], [5], [6] to extract the nanostructure profiles by solving the inverse problem [7], [8], [9]. In this inverse problem, the predicted signature, calculated by a trial shape function, is compared to the measured signature. The trial shape undergoes modulation until the predicted signature closely matches the observed one.

Measurement errors are inevitable in any metrology, introducing uncertainties in the measured results. To enhance the reliability of the measured results, it is essential to consider not only the accuracy but also the precision of the measured results. The accuracy reflects the influence of systematic error, while the precision reflects the influence of random error. The error propagation theory is applicable for evaluating parameter uncertainties when explicit knowledge of measurement error sources is available. For instance, if measurement errors follow a Gauss distribution, parameter uncertainties can be assessed by extracting the square root of the main diagonal entries from the covariance matrix of the parameters. This approach is commonly utilized for uncertainty evaluation in optical CD (OCD) [10], [11]. However, it is not applicable to CD-SAXS, as the measurement accounts for Poisson statistical noise associated with complex error sources, such as the divergence of the incident beam and the inhomogeneity of the detector [12]. It appears to be a myth that considers all known or suspected error components and evaluates them correctly and appropriately by the error propagation theory.

According to the Guide to the Expression of Uncertainty in Measurement (GUM), a powerful technique to characterize the uncertainties of parameters directly and simply is the sampling method [13]. The Markov chain Monte Carlo (MCMC) method is popular in CD-SAXS for assessing parameter uncertainties [14], [15], [16], [17]. It generates a population of models to estimate parameter uncertainties. This is accomplished by an initial model, generally the best-known fit, and then introducing random perturbations to the initial model for model updating. The updated model is accepted or rejected based on the change in the goodness-of-fit (GoF) metric. If the current GoF is smaller than the previous one, the updated model is accepted into the population. Otherwise, a weighted probability P is calculated, and a random variable α is generated from the interval [0, 1]. The acceptance or rejection of the updated model is then determined by comparing P and α. This process is repeated until a sufficient number of accepted models in the population reach equilibrium. While MCMC is widely adopted in CD-SAXS, it requires good initial values,

Received 23 May 2024; revised 19 August 2024; accepted 23 August 2024. Date of publication 11 September 2024; date of current version 24 September 2024. This work was supported in part by the National Natural Science Foundation of China under Grant 52022034, Grant 62175075, and Grant 52130504; in part by the National Key Research and Development Plan of China under Grant 2022YFF0709104; in part by the Key Research and Development Plan of Hubei Province under Grant 2020BAA008; and in part by the Innovation Project of Optics Valley Laboratory under Grant OVL2023PY003. The Associate Editor coordinating the review process was Dr. Rosenda Valdes Arencibia. *(Corresponding authors: Xiuguo Chen; Shiyuan Liu.)*

Tianjuan Yang, Shuo Liu, and Jiahao Zhang are with the State Key Laboratory of Intelligent Manufacturing Equipment and Technology, Huazhong University of Science and Technology, Wuhan 430074, China (e-mail: tianjuanyang@hust.edu.cn).

Xiuguo Chen and Shiyuan Liu are with the State Key Laboratory of Intelligent Manufacturing Equipment and Technology and Optics Valley Laboratory, Huazhong University of Science and Technology, Wuhan 430074, China (e-mail: xiuguochen@hust.edu.cn; shyliu@hust.edu.cn).

Digital Object Identifier 10.1109/TIM.2024.3458063

broad parameter boundaries, and multiple independent chains to guarantee algorithm convergence. Meanwhile, it is unable to distinguish some defective or invalid samples, resulting in larger uncertainty estimates [9]. Furthermore, the choice of weighted probability significantly influences parameter acceptance and rejection, thereby impacting uncertainty evaluation. The determination of the parameter step size also warrants careful consideration in MCMC. A large step may cause significant jumps in model parameters, resulting in a low acceptance rate, while a small step may lead to prolonged wandering in the parameter space, reducing efficiency. Therefore, it is of great significance to develop a more convenient and effective uncertainty evaluation method that can account for complex error sources. Such a method would be a valuable supplement to existing uncertainty evaluation methods in CD-SAXS.

Bootstrap method emerges as a powerful sampling method that allows for Monte Carlo simulations based on the actual data in hand, and making inferences from those data. This method maximizes the utilization of existing data without necessitating additional model assumptions or the acquisition of new data [18], [19]. It exhibits robustness and simplicity, making it extensively employed in many fields such as machine learning, especially in situations, where understanding of the underlying process or measurement errors is limited. However, the application of the bootstrap method in IC metrology is not widespread. One possible reason is the existence of numerous bootstrap methods, each with its distinct strengths and weaknesses, which may not be clear to nonstatisticians. Another reason could be the relatively slower nature of the bootstrap method in solving inverse problems compared to the error propagation theory-based uncertainty analysis approach. The earlier work on applying the bootstrap method in IC metrology was implemented in ellipsometry [20], subsequently followed by several studies, as referenced in [21] and [22]. While the application of the bootstrap method in CD-SAXS is rarely mentioned. As described in previous work [20], the parameter uncertainty was estimated using the bootstrap percentile method simply and naturally, which relies on the assumption of a symmetric distribution. However, this can introduce bias or inaccuracy when dealing with asymmetric distribution.

In this work, we present a new version of the bootstrap method to address the inverse problem of CD-SAXS by bootstrapping measured data (i.e., the measured intensity), calculating their mean values, and subsequently using these mean values to solve the inverse problem and obtain a bootstrap estimate. Furthermore, we introduce a centered bootstrap percentile method and incorporate a bias correction procedure to enhance the accuracy of measurement results, specifically considering the skewed distribution observed in CD-SAXS. Subsequently, we conduct simulations and measurements using both 1-D and 2-D gratings. The accuracy of the method is verified by comparing the extracted parameters with those obtained from OCD. Furthermore, the precision of the method is verified by comparing the parameter uncertainties with those obtained from MCMC. We should emphasize that the proposed method is not limited to CD-SAXS metrology but also holds applicability in other related model-based measurement techniques.

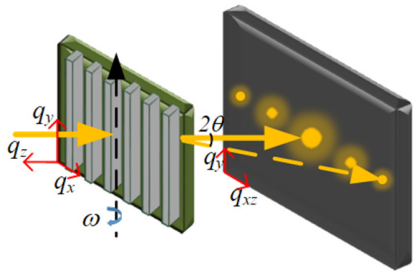

Fig. 1. Schematic for the CD-SAXS geometry illustrating the scattering angle 2θ, the rotation angle ω, and the definitions of the q vectors for both the nanostructure and the detector.

The remainder of this article is organized as follows. In Section II, we begin by briefly introducing the inverse problem of CD-SAXS. Following that, we present the proposed bootstrap method and apply it to the inverse problem of CD-SAXS. In Sections III and IV, we provide some simulated and experimental results, along with discussions, to illustrate the validity of the proposed method. Section V gives some conclusions.

II. Methodology

A. CD-SAXS Metrology

The schematic for CD-SAXS measurement is illustrated in Fig. 1. The nanostructure is positioned on a rotation stage, with the line grating aligned parallel to the rotation axis. X-rays impinge on the nanostructure and scatter at small angles of the primary beam. The scattering intensity I is recorded as a function of the scattering vector $\boldsymbol{q} = 4\pi \sin\theta/\lambda$, where 2θ represents the scattering angle, and λ denotes the wavelength. The definitions of the $\boldsymbol{q}$ vectors for both the nanostructure (q_x, q_y, q_z) and the detector (q_{xz}, q_y) are provided in Fig. 1. The nanostructure is rotated at a series of angles to generate a reciprocal space map (RSM). The inverse problem is addressed by selectively fitting the scattering intensity I versus q_z at each diffraction order (referred to as q_z slice), or by fitting the scattering intensity I versus q_{xz} at each rotation angle ω, resulting in the extraction of nanostructure parameters [5].

A general outline of the process for solving the inverse problem is depicted in Fig. 2. The main steps include the following.

1) Collecting the measured intensity $\boldsymbol{I}_{\text{meas}}$ of the nanostructure.
2) Parameterizing the profile of the nanostructure under test and establishing a forward model to calculate the predicted intensity related to the profile. Generally, the predicted intensity $\boldsymbol{I}_{\text{sim}}$ is calculated using (1) and (2) [9]. The scattering intensity $\tilde{\boldsymbol{I}}_{\text{sim}}$ is calculated through the Fourier transform of the scattering length density profile, cf. (1), where $\rho(r)$ represents the shape function including electron density contrast. Here, L denotes the pitch, l represents the dimension along the pitch, and $*$ indicates the convolution. Subsequently, a scaling factor $\boldsymbol{I}_s$, a Debye–Waller factor DW,

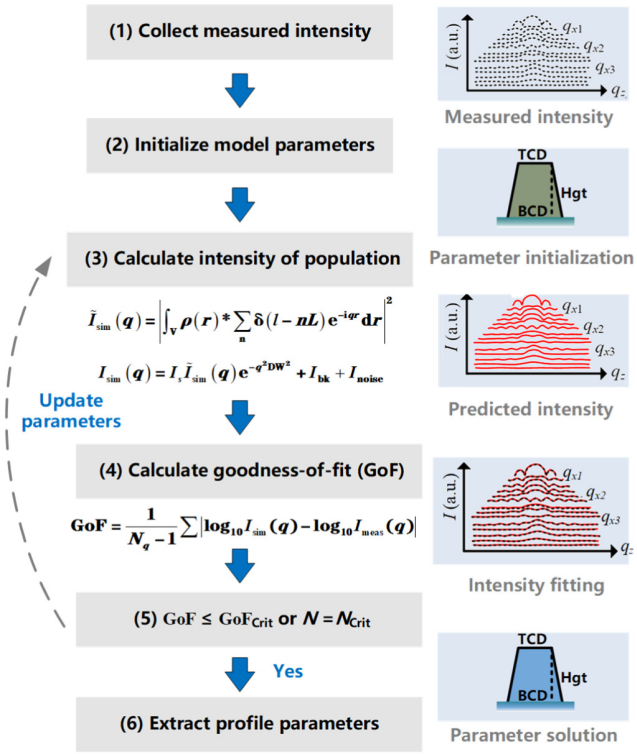

Fig. 2. Flowchart of the inverse problem in CD-SAXS.

an average background term $\boldsymbol{I}_{\text{bk}}$, and a Poisson noise $\boldsymbol{I}_{\text{noise}}$ are incorporated to align the predicted intensity with the experimental data, as shown in (2).

3) Performing the intensity fitting procedure using an optimization algorithm such as a genetic algorithm, to extract nanostructure parameters r. This step is repeated until a convergence criterion is reached, either when the GoF is less than or equal to a predetermined threshold goodness-of-fit (GoF_{Crit}) ($\text{GoF} \leq \text{GoF}_{\text{Crit}}$) or when the number of iterations reaches a preset limit ($N = N_{\text{Crit}}$)

$$\tilde{\boldsymbol{I}}_{\text{sim}}(\boldsymbol{q}) = \left| \int_V \rho(\boldsymbol{r}) * \sum_n \delta(l - nL) e^{-i\boldsymbol{q}\boldsymbol{r}} d\mathbf{r} \right|^2 \tag{1}$$

$$\boldsymbol{I}_{\text{sim}}(\boldsymbol{q}) = \boldsymbol{I}_s \tilde{\boldsymbol{I}}_{\text{sim}}(\boldsymbol{q}) \times e^{-\boldsymbol{q}^2 DW^2} + \boldsymbol{I}_{\text{bk}} + \boldsymbol{I}_{\text{noise}}. \tag{2}$$

To extract an optimal set of parameters, it is necessary to select an objective function that effectively captures the GoF. In this work, we adopt a standard objective function that compares the mean absolute error (MAE) between the logarithmic values of the measured and predicted intensities, as detailed in [9]. The specific form of this objective function used is as follows:

$$\text{GoF} = \frac{1}{N_q - 1} \sum \left| \log_{10} \boldsymbol{I}_{\text{sim}}(q) - \log_{10} \boldsymbol{I}_{\text{meas}}(q) \right| \tag{3}$$

where N_q is the number of measured data, $\boldsymbol{I}_{\text{sim}}$ is the predicted intensity, and $\boldsymbol{I}_{\text{meas}}$ is the measured intensity. This objective function is well suited for situations, where the data span many orders of magnitude, as is often the case with scattering intensity data, where the primary peak can be significantly larger than the high peak.

B. Bootstrap Method for the Inverse Problem

The bootstrap method is based on the plug-in principle to obtain the estimates when other methods are failed [18]. To enhance the accuracy of measurement results, it is a common practice to repeat the measurement multiple times and obtain the results by calculating the averages of the extracted parameters. As the number of measurements increases indefinitely, the average is considered the closest to the true value. However, in practice, only a finite number of measurements can be obtained. The bootstrap method offers a way to utilize the measured data at hand to not only approximate the desired quantity but also obtain the associated uncertainty. Fig. 3 illustrates the general flow of the bootstrap method. Suppose that the parameter r is some interesting estimate of the population I, such as mean, variance, proportion, or other characteristics of the population. We denote the statistical operation F as the function that transforms the population I to the estimate r. The original sample $\boldsymbol{I}_0$ with N observed data $\boldsymbol{I}_{0i}$ $(i = 1, 2, \ldots, N)$ is distributed according to the population I, and suppose the corresponding estimate computed from this original sample is $\hat{\boldsymbol{r}}$. The idea behind the bootstrap method is to summarize the distribution of r based on studying the distribution of $\hat{\boldsymbol{r}}$ using the observed data at hand. To do this, the bootstrap method follows a prescribed process: First, several bootstrap samples, $\boldsymbol{I}_1, \boldsymbol{I}_2, \ldots, \boldsymbol{I}_B$, are generated. Each bootstrap sample $\boldsymbol{I}_m$ consists of N data points $\boldsymbol{I}^*_{mi}$ $(m = 1, 2, \ldots, B$ and $i = 1, 2, \ldots, N)$ drawn with replacement from the original sample I_0. Due to this replacement, some observed data I_{0i} $(i = 1, 2, \ldots, N)$ may appear multiple times or not at all in each bootstrap sample. Subsequently, the corresponding estimates $\hat{\boldsymbol{r}}^*_m$ are computed from each bootstrap sample. Finally, a histogram of the bootstrap distribution of the estimates $\hat{\boldsymbol{r}}^*_m$ can be constructed. Bootstrap method points out that the variability of $\hat{\boldsymbol{r}}$ around r can be mimicked by the variability of $\hat{\boldsymbol{r}}^*_m$ around $\hat{\boldsymbol{r}}$ [19].

In this work, we introduce a new version of the bootstrap method on the inverse problem of CD-SAXS. The approach is defined as follows.

1) Generate an "original sample" $\boldsymbol{I}_0 = \{\boldsymbol{I}_{01}, \boldsymbol{I}_{02}, \ldots, \boldsymbol{I}_{0N}\}$ that comprises N sets of measured data from N repeated measurements, with each $\boldsymbol{I}_{0i}$ $(i = 1, 2, \ldots, N)$ being a vector of measured intensity.
2) Compute the average of this original sample $\boldsymbol{I}_0 = \{\boldsymbol{I}_{01}, \boldsymbol{I}_{02}, \ldots, \boldsymbol{I}_{0N}\}$ to obtain the average data $\tilde{\boldsymbol{I}}_0$, which is of the same size as $\boldsymbol{I}_{01}, \boldsymbol{I}_{02}, \ldots, \boldsymbol{I}_{0N}$. Then, solve the inverse problem using the average data $\tilde{\boldsymbol{I}}_0$ to obtain an original estimate $\hat{\boldsymbol{r}}$, i.e., the extracted parameters. In this way, the traditional concept of the bootstrap method has been extended, allowing the statistical operation F to be generalized from conventional operations such as mean, variance, and median, to encompass the mean and inverse problem-solving operations demonstrated in this work.
3) By drawing with replacement from $\boldsymbol{I}_0$ N times, a bootstrap sample $\boldsymbol{I}_1 = \{\boldsymbol{I}^*_{11}, \ldots, \boldsymbol{I}^*_{1N}\}$ is obtained, with each $\boldsymbol{I}^*_{1i}$ $(i = 1, 2, \ldots, N)$ being one of $\boldsymbol{I}_{01}, \boldsymbol{I}_{02}, \ldots, \boldsymbol{I}_{0N}$.
4) Compute the average of this bootstrap sample $\boldsymbol{I}_1 = \{\boldsymbol{I}^*_{11}, \ldots, \boldsymbol{I}^*_{1N}\}$ to obtain the average data $\tilde{\boldsymbol{I}}_1$. Then, solve

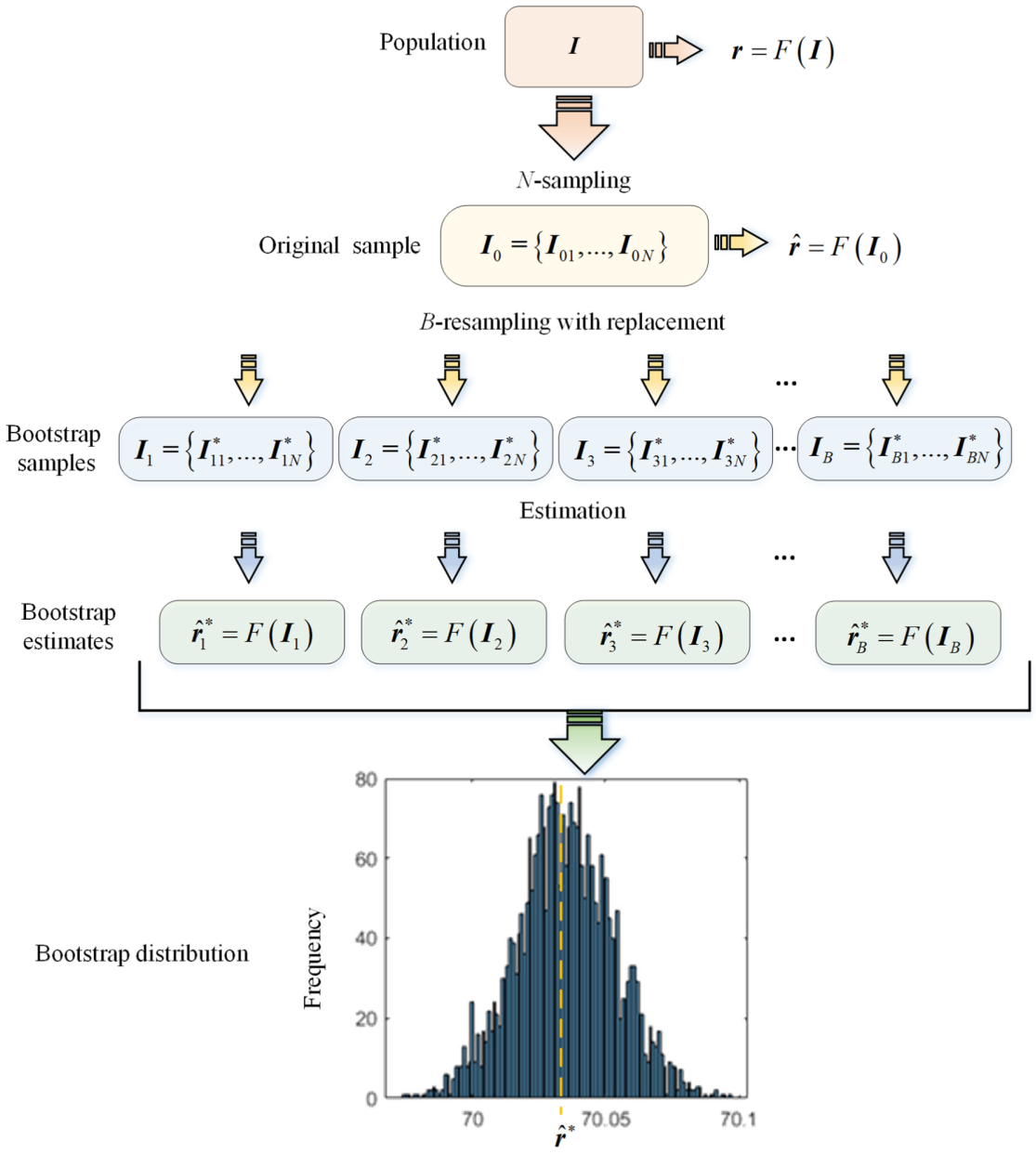

Fig. 3. Flowchart of the bootstrap method.

the inverse problem using the average $\tilde{I}_1$ to obtain a bootstrap estimate $\hat{r}_1^*$.

5) Repeat the above Steps 3 and 4 B times, generating B sets of bootstrap estimates: $\{\hat{r}_1^*, \hat{r}_2^*, \ldots, \hat{r}_B^*\}$.
6) Rank these bootstrap estimates in ascending order, obtaining an order $\{\hat{r}_{(1)}^*, \hat{r}_{(2)}^*, \ldots, \hat{r}_{(B)}^*\}$.
7) Compute the average of these bootstrap estimates, obtaining the final extracted parameters

$$\hat{r}^* = \frac{\sum_{m=1}^{B} \hat{r}_m^*}{B}. \tag{4}$$

The determination of the confidence interval conventionally relies on the bootstrap percentile method

$$r_{\alpha/2}^* \le r \le r_{1-\alpha/2}^* \tag{5}$$

where r_α^* denotes the α-percentile of the distribution of $\hat{r}_{(m)}^*(m = 1, 2, \ldots, B)$. However, this estimation is associated with a symmetrical distribution, which is not commonly observed in CD-SAXS. To address this, we adopt a more suitable centered bootstrap percentile method and employ a bias correction procedure, if necessary, to achieve more accurate results. The centered bootstrap confidence interval is based on the bootstrap sampling principle, this means that we could obtain the distribution of $\hat{r} - r$ robustly by those of $\hat{r}_{(m)}^* - \hat{r}$. Suppose that s_α^* denotes the α-percentile of the distribution of $\hat{r} - r$, and then, a probability statement for $\hat{r} - r$ is

$$P\left(s_{\alpha/2}^* \le \hat{r} - r \le s_{1-\alpha/2}^*\right) = 1 - \alpha. \tag{6}$$

After rearranging, we get the following interval:

$$\hat{r} - s_{1-\alpha/2}^* \le r \le \hat{r} - s_{\alpha/2}^*. \tag{7}$$

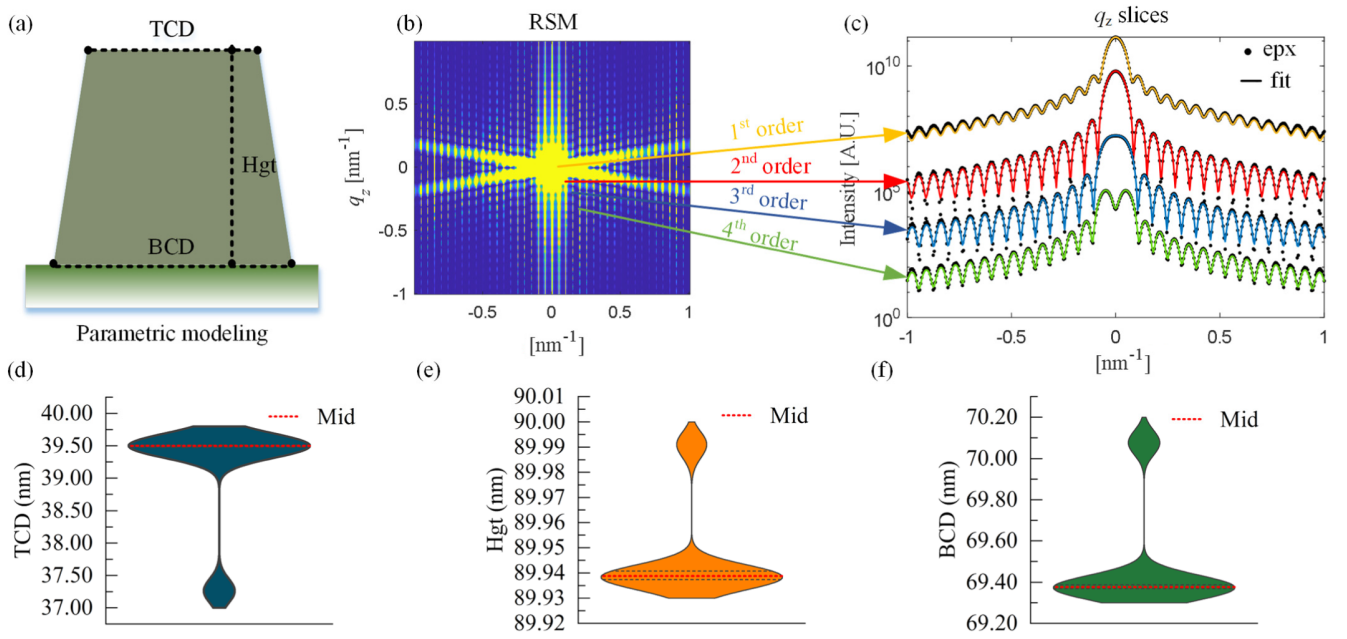

Fig. 4. (a) Model parameterization of the grating. (b) Simulated RSM of grating. (c) Fitting results of the q_z slices in the inverse problem of CD-SAXS (intensities are arbitrarily scaled for visualization). (d)–(f) Violin plots representing the bootstrap distributions of three parameters of TCD, Hgt, and BCD, respectively. The median value is indicated by the dotted red line.

If $\boldsymbol{r}^*_\alpha$ denotes the α-percentile of the distribution of $\hat{\boldsymbol{r}}^*_{(m)}$ and $\boldsymbol{s}^*_\alpha$ of $\hat{\boldsymbol{r}}^*_{(m)} - \hat{\boldsymbol{r}}$, then $\boldsymbol{s}^*_\alpha$ is related to $\boldsymbol{r}^*_\alpha$ by

$$\boldsymbol{s}^*_\alpha = \boldsymbol{r}^*_\alpha - \hat{\boldsymbol{r}}. \tag{8}$$

Inserting (8) into (7) gives

$$2\hat{\boldsymbol{r}} - \boldsymbol{r}^*_{1-\alpha/2} \le \boldsymbol{r} \le 2\hat{\boldsymbol{r}} - \boldsymbol{r}^*_{\alpha/2}. \tag{9}$$

The estimate of the standard uncertainty can be defined as half the length of this interval

$$\begin{aligned}\boldsymbol{\sigma} &= 2\hat{\boldsymbol{r}} - \boldsymbol{r}^*_{\alpha/2} - \left(2\hat{\boldsymbol{r}} - \boldsymbol{r}^*_{1-\alpha/2}\right) \\ &= \boldsymbol{r}^*_{1-\alpha/2} - \boldsymbol{r}^*_{\alpha/2}.\end{aligned} \tag{10}$$

Comparing (5) and (10), we can observe that the two estimation methods differ only by an offset for confidence interval estimation, which does not impact the estimate of uncertainty. We emphasize that the centered bootstrap method is suitable for both symmetric and asymmetric distributions, adhering to the principles of the bootstrap method. This approach is particularly well suited for accurately capturing the skewness of the distribution.

In addition to the bias of the interval, the point estimate $\hat{\boldsymbol{r}}^*$ could also exhibit bias when using (4), which may exceed the confidence interval. If this happens, the following bootstrap-based approximation for this bias can be taken:

$$\widehat{\text{bias}}_B = \hat{\boldsymbol{r}}^* - \hat{\boldsymbol{r}} \tag{11}$$

i.e., the difference between the average of the bootstrap estimate and the original estimate. Then, the following corrected bootstrap estimate can be used [18]:

$$\hat{\boldsymbol{r}}^*_c = \hat{\boldsymbol{r}} - \widehat{\text{bias}}_B = 2\hat{\boldsymbol{r}} - \hat{\boldsymbol{r}}^*. \tag{12}$$

III. Simulation

To validate the effectiveness of the proposed bootstrap method in CD-SAXS, we conducted a simulation on 1-D grating and analyzed the bootstrap estimates obtained from CD-SAXS. The grating is characterized by a symmetrical trapezoidal model with top CD (TCD), grating height (Hgt), bottom CD (BCD), and a fixed period of 125 nm, as illustrated in Fig. 4(a). The nominal dimensions of the testing sample are TCD = 37 nm, Hgt = 91 nm, and BCD = 70 nm. We should note that the proposed method is not limited to the investigated sample and can be readily used for complex nanostructures with more structural parameters under measurement.

In CD-SAXS simulation, the predicted intensity is generated from the forward model and then transformed into the "measured" one by adding the following Poisson noise [9]:

$$\zeta(\boldsymbol{q}) = \sqrt{I_{\text{sim}}(\boldsymbol{q})/6I_{\text{bk}}}\,\text{rand}([-1, 1]). \tag{13}$$

Given that the Poisson noise is proportional to the square root of the observed intensity. Here, I_{sim} represents the predicted intensity, and I_{bk} corresponds to the background scattering intensity. Fig. 4(b) depicts the intensity distribution with q_x and q_z values ranging from -1 to 1 nm^{-1}. Blue areas signify low-intensity regions, while yellow areas indicate high-intensity regions. In the simulation, we performed five repeated "measurements" by randomly generating five groups of "measured" data using (13) to obtain the original sample $\boldsymbol{I}_0$ in the bootstrap method. Fig. 4(c) presents the fitting results using q_z slices at q_x diffraction orders ranging from 1 to 4, obtained from the average of the original sample $\boldsymbol{I}_0$ using a genetic algorithm. The intensities are arbitrarily scaled for visualization. Following the acquisition of the original sample $\boldsymbol{I}_0$, the bootstrap method was implemented according to the aforementioned procedure. While there are no strict

TABLE I
BOOTSTRAP ESTIMATIONS OF THREE PARAMETERS OBTAINED FROM CD-SAXS

	TCD (nm)	Hgt (nm)	BCD (nm)
μ_1	39.98	89.93	69.28
μ_2	38.99	89.95	69.54
σ_1	1.210	0.035	0.357
σ_2	2.381	2.244	2.619

guidelines for selecting the bootstrap number B, it is generally advised to increase B rather than decrease B, as the observed sample size grows [18]. The general recommendation of the bootstrap number is 100–500. In this work, we adopted a bootstrap number of $B = 500$.

Fig. 4(d)–(f) illustrates the bootstrap distributions of three parameters (TCD, Hgt, and BCD). It is evident that, under the Poisson noise model, the bootstrap distributions are asymmetrical and mainly distributed in two intervals for each parameter. Therefore, the centered bootstrap percentile method is suitable, and we employed a bias correction procedure. In addition, we assessed the parameter uncertainties obtained from MCMC for comparison. In this study, we typically employed 50 chains with 100 000 steps in the MCMC method, and the chains were resampled every 50 steps to remove interchain correlations. The weighted probability of accepting the model is determined by the following equation:

$$\mathrm{P}_i = \mathrm{e}^{-0.5(\mathrm{GoF}_i - \mathrm{GoF}_{i-1})}. \tag{14}$$

Additional details of the MCMC have been described previously [9].

Table I provides the mean values of three parameters associated with their uncertainties (with a confidence level of 95%) obtained from different methods. It is observed that under the influence of Poisson noise, the extracted parameters obtained from both the centered bootstrap percentile method (μ_1) and the bootstrap percentile method (μ_2) deviate from the nominal values [37, 91, 70] nm, with a notable difference in TCD (a deviation of 2.98 nm for μ_1 and 1.99 nm for μ_2) and a minor difference in BCD (a deviation of 0.72 nm for μ_1 and 0.46 nm for μ_2). The differences between the uncorrected mean values (μ_2) and the corrected mean values (μ_1) of the three parameters are minimal, with a notable difference in TCD ($\sim$1 nm) and a minor difference in Hgt (0.02 nm). However, the uncorrected mean values (μ_2) exceed the confidence interval due to the skewed distribution. Specifically, the uncorrected mean value of TCD is 38.99 nm, falling outside the 95% confidence interval [39.45, 41.87] nm, while the corrected mean value is 39.98 nm, falling within the confidence interval. Similarly, for the BCD parameter, the uncorrected mean value is 69.54 nm, falling outside the 95% confidence interval [68.74, 69.46] nm, while the corrected mean value is 69.28 nm, falling within the confidence interval. This demonstrates the effectiveness of the proposed bootstrap method in accurately capturing the skewness of the distribution.

By comparing the parameter uncertainties estimated by the proposed bootstrap method (σ_1) and the MCMC method (σ_2), it can be observed that the uncertainties of three parameters estimated by the MCMC method show relatively small differences, while the uncertainties estimated by the proposed method show relatively large differences. In addition, the parameter uncertainties estimated by the MCMC method are larger than those estimated by the bootstrap method. Specifically for BCD, although its mean closely approaches the nominal value, the uncertainty estimated by the MCMC method remains large. As previously discussed, the MCMC method does not inherently distinguish potential defect samples, while the proposed bootstrap method can comprehensively capture the variability in the measurement, offering a more thorough evaluation. This simulation demonstrates the effectiveness of the proposed bootstrap method in addressing the inverse problem of CD-SAXS, obtaining both the mean values of parameters and their associated uncertainties.

IV. EXPERIMENT

To further validate the proposed method, we carried out a series of repeated experiments on a 1-D Si grating and a 2-D cylindrical Si grating. Subsequently, we analyzed the bootstrap estimates obtained from these CD-SAXS measurements. To validate the accuracy of the proposed bootstrap method, we compared the extracted parameters obtained from OCD. The OCD measurement was conducted using an industrial dual-rotating-compensator Mueller matrix scatterometry (ME-L, Wuhan Eoptics Technology Company China) [23], [24]. The spectral range varied from 200 to 800 nm with increments of 10 nm. The full 15 Mueller matrix elements can be obtained and normalized by the first element. To validate the precision of the proposed method, we compared the parameter uncertainties estimated by MCMC.

CD-SAXS measurements were performed at the small-angle X-ray scattering (SAXS) beamline of the Shanghai Synchrotron Radiation Facility (SSRF) [25]. The data were collected by transmitting X-rays through the silicon substrate with an energy of 10 keV. Scattered X-rays were collected on a 2-D detector (Pilatus 2 M) with a sample-to-detector distance of 1.97 m. Due to the limitations of experimental conditions, the repeated measurements were conducted only at 0° and 30° incidence angles for the 1-D Si grating and 0° incidence angle for the 2-D Si grating. Despite the constrained incidence angles, satisfactory fitting results were still achieved due to the relatively simple profiles of these two samples and good prior knowledge of the samples.

Fig. 5(a) provides the SEM image and parametric modeling of the 1-D grating used for analyzing the bootstrap estimates in CD-SAXS measurements. The SEM image reveals that the local width of the grating structure is 61.26 nm. However, SEM only captures local features of the structure under test and does not provide the average size of the structure. In contrast, CD-SAXS and OCD can provide statistical

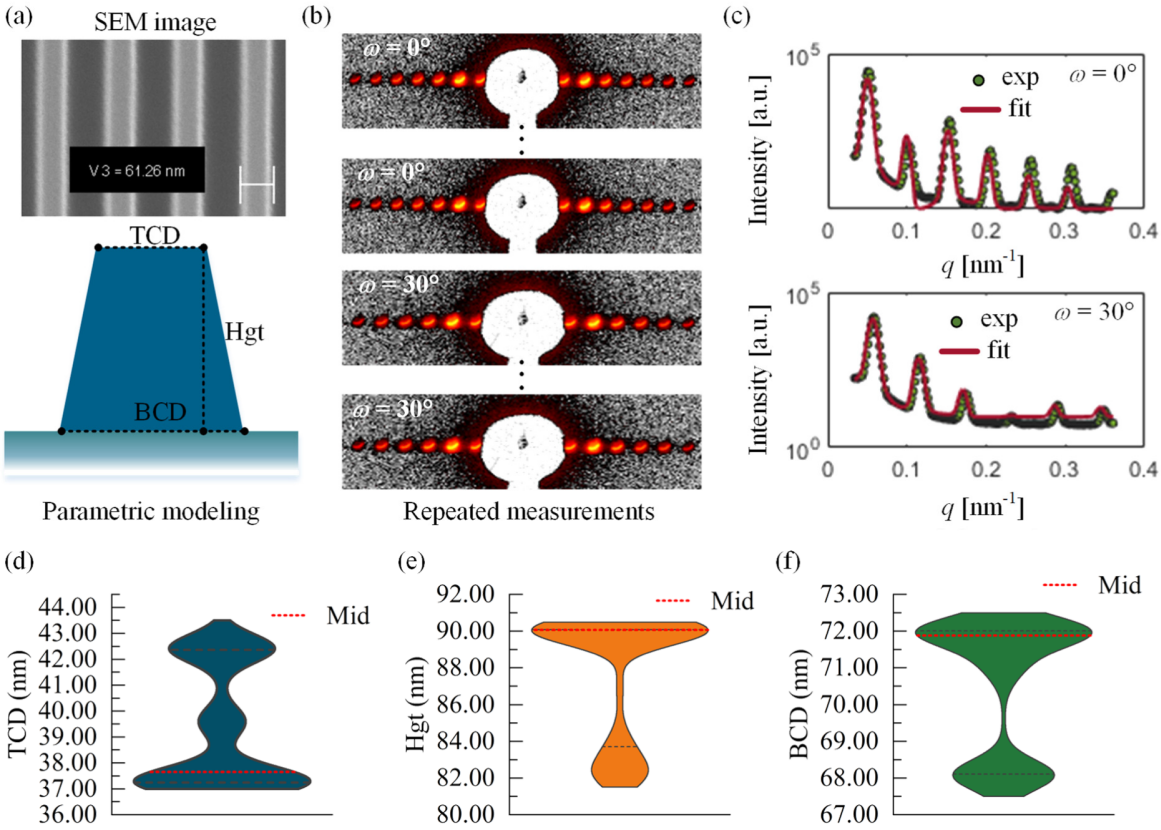

Fig. 5. (a) SEM image and parametric modeling of the 1-D Si grating. (b) Subset of scattering patterns obtained from five repeated CD-SAXS measurements at two incident angles. (c) Fitting results of the measured and predicted intensities at two incident angles. (d)–(f) Violin plots representing the bootstrap distributions of three parameters of TCD, Hgt, and BCD, respectively. The median value is indicated by the dotted red line.

information about the structure under test within the illuminated area [2]. Fig. 5(b) displays a subset of scattering patterns from five repeated measurements at incidence angles of 0° and 30°, respectively. Fig. 5(c) presents the fitting results of the measured and predicted intensities obtained from the average of the five repeated measurements under two incidence angles. Fig. 5(d)–(f) illustrates the bootstrap distributions of three parameters (TCD, Hgt, and BCD). Similar to the Poisson noise assumed in the simulation, the bootstrap distributions are asymmetrical. Therefore, the centered bootstrap percentile method is suitable, and a bias correction procedure is employed to correct the mean values and prevent them from exceeding the confidence interval.

Fig. 6 presents the OCD fitting results of the measured spectra and the predicted spectra for the 1-D Si grating at the measurement configuration of incident angle $\theta = 65°$ and azimuth angle $\varphi = 30°$. The fitting results show a good match.

Table II provides extracted parameters associated with their uncertainties (with a confidence level of 95%) obtained from different methods. The extracted parameters obtained from CD-SAXS (μ_1) and OCD (μ_2) align closely, with a maximum difference of 1.88 nm in TCD and a minimum difference of 0.98 nm in BCD. The results demonstrate the feasibility and accuracy of the proposed bootstrap method in estimating mean values in CD-SAXS. Table II also presents the parameter uncertainties estimated by the proposed bootstrap method (σ_1) and the MCMC method (σ_2). The parameter uncertainties estimated by the two methods are relatively consistent, demonstrating the feasibility and precision of the proposed bootstrap method in evaluating parameter uncertainties in CD-SAXS.

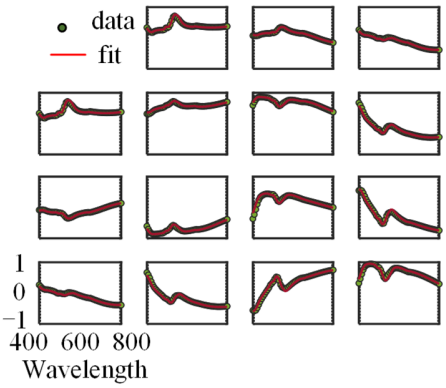

Fig. 6. Fitting results of the measured and calculated Mueller matrix spectra of 1-D Si grating.

TABLE II
EXTRACT PARAMETERS AND UNCERTAINTIES OF 1-D Si GRATING OBTAINED FROM DIFFERENT METHODS

	TCD (nm)	Hgt (nm)	BCD (nm)
μ_1	35.11	93.07	72.42
μ_2	36.99	91.40	71.44
σ_1	2.464	2.511	1.782
σ_2	2.169	2.529	2.007

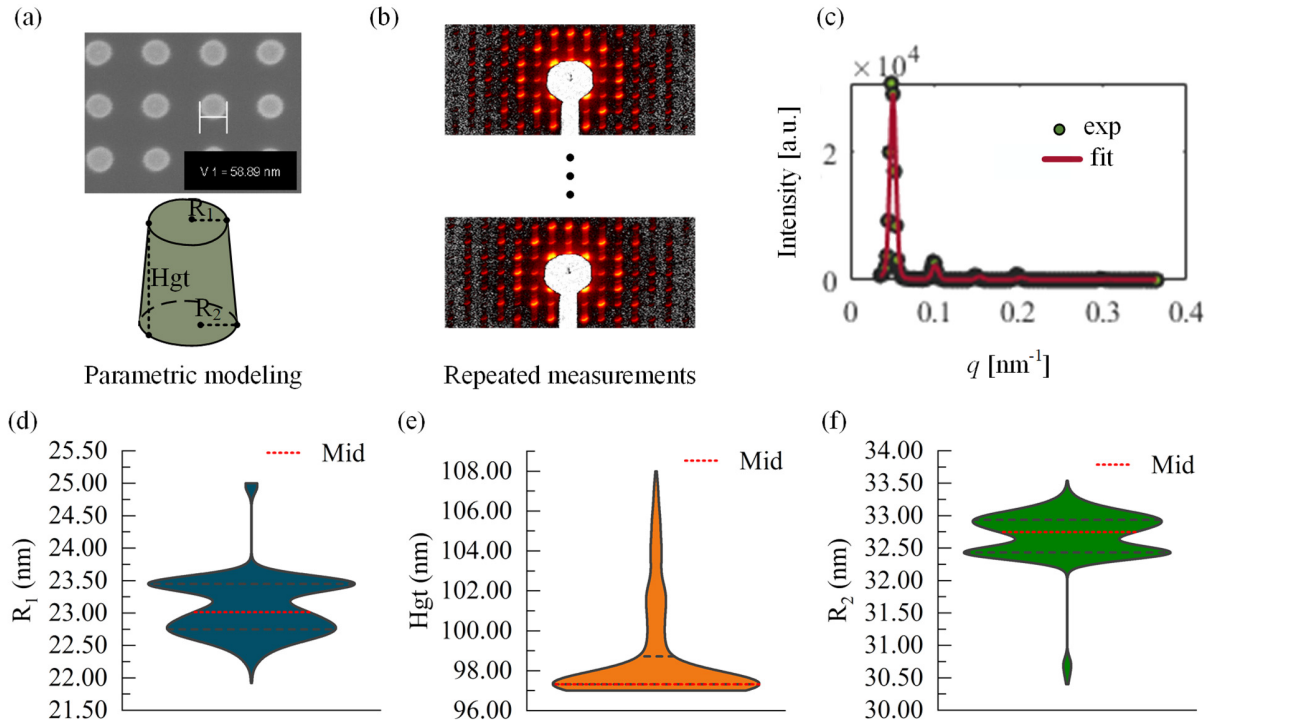

Fig. 7. (a) SEM image and parametric modeling of the 2-D cylindrical grating. (b) Subset of scattering patterns of five repeated CD-SAXS measurements. (c) Fitting results of the measured and calculated intensities obtained from the average data of five repeated measurements. (d)–(f) Violin plots representing the bootstrap distributions of three parameters of R_1, Hgt, and R_2, respectively. The median value is indicated by the dotted red line.

Fig. 7(a) provides the SEM image and parametric modeling of the 2-D cylindrical grating used for analyzing the bootstrap estimates in CD-SAXS measurements. Fig. 7(b) displays a subset of scattering patterns from five repeated measurements at normal incidence. Fig. 7(c) presents the fitting results of the measured and predicted intensities obtained from the average of the five repeated measurements. The bootstrap method was employed to obtain the mean values and uncertainties of the parameters. Fig. 7(d)–(f) illustrates the bootstrap distributions of three parameters (R_1, Hgt, and R_2). Similarly, the bootstrap distributions are asymmetrical and spread across large intervals for three parameters. Therefore, we employed the centered bootstrap percentile method and a bias correction procedure to correct the mean values and prevent them from exceeding the confidence interval.

For comparison, OCD measurements were also conducted on the 2-D cylindrical grating. Fig. 8 presents the fitting results of the measured spectra and the predicted spectra for the grating at the measurement configuration of incident angle $\theta = 65°$ and azimuth angle $\varphi = 60°$, the fitting results exhibit a good match.

Table III provides extracted parameters associated with their uncertainties (with a confidence level of 95%) obtained from different methods. The extracted parameters obtained from CD-SAXS (μ_1) and OCD (μ_2) align with each other, with a maximum difference of 3.75 nm in Hgt and a minimum difference of 2.96 nm in R_1. In addition to the differences in extracted parameters resulting from the utilization of different metrologies, another factor may stem from our utilization of measured data obtained from only one incidence angle in CD-SAXS.

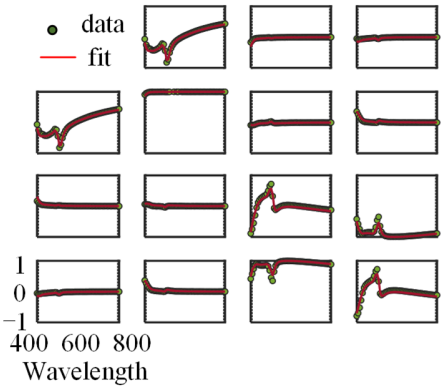

Fig. 8. Fitting results of the measured and calculated Mueller matrix spectra of 2-D Si grating.

TABLE III
EXTRACT PARAMETERS AND UNCERTAINTIES OF 2-D Si GRATING OBTAINED FROM DIFFERENT METHODS

	R_1 (nm)	Hgt (nm)	R_2(nm)
μ_1	22.96	102.95	32.61
μ_2	20.00	106.70	29.50
σ_1	0.589	3.000	0.385
σ_2	2.644	2.839	2.903

Table III also presents the parameter uncertainties estimated by the proposed bootstrap method (σ_1) and the MCMC method (σ_2). It is observed that the uncertainties estimated by the MCMC method show relatively small differences, while the uncertainties estimated by the proposed method show

relatively large differences. In addition, the parameter uncertainties estimated by the MCMC method are larger than those estimated by the bootstrap method, except for Hgt. The larger uncertainty of Hgt in CD-SAXS can be attributed to the fact that its mean value differs more significantly from the value obtained from OCD, resulting in relatively greater uncertainty. This further demonstrates the effectiveness of the proposed bootstrap method in solving the inverse problem of CD-SAXS. The proposed bootstrap method can comprehensively capture the variability in the measurement, offering a more thorough evaluation. It can provide both the mean values of parameters and their associated uncertainties without any explicit analysis of error source and error propagation.

V. Conclusion

The application of the bootstrap method in the inverse problem of CD-SAXS has showcased its capability to assess both the mean values of parameters and the associated uncertainties by leveraging measured data, serving as a supplement to the existing evaluation methods in CD-SAXS. The full article is summarized as follows.

1) A new version of the bootstrap method is designed by bootstrapping measured data, i.e., the measured intensity, calculating their mean values, and then solving the inverse problem using these mean values to obtain a bootstrap estimate. In this way, the traditional concept of the bootstrap method has been extended, allowing the statistical operation F to be generalized from conventional operations such as mean, variance, and median, to encompass the mean and inverse problem-solving operations demonstrated in this work.
2) Based on the bootstrap principle, a more appropriate centered bootstrap percentile method is adopted in the inverse problem of CD-SAXS along with a bias correction procedure to achieve more accurate results, suitable for both normal and nonnormal distribution situations.
3) Simulations and experiments are conducted on both 1-D and 2-D Si gratings. The accuracy of the proposed method is verified by comparison with OCD, and the precision of the proposed method is verified by comparison with the MCMC method. The results demonstrate that the MCMC method does not inherently distinguish potential defect samples, while the proposed bootstrap method can comprehensively capture the variability in the measurement, providing a more thorough evaluation and obtaining both the mean values of parameters and their associated uncertainties without any explicit analysis of error source and error propagation. The proposed method significantly broadens the uncertainty evaluation methods in CD-SAXS, OCD, and other model-based measurement techniques.

It should be noted that the accuracy of the estimate is influenced by the size of the original sample. Therefore, a careful selection of sample size is crucial to ensure the reliability of the results. Due to the limited measurement time and sufficient prior knowledge about the tested nanostructure, only five repeated measurements were conducted. Despite employing just five sets of original samples in this study, reasonable results were obtained and that does the trick. Moreover, the bootstrap method employed in this work does not explicitly consider the data interdependence or identify outliers during the resampling process. For future research, it is worth considering the utilization of the parametric bootstrap method or the integration of data outlier detection techniques in the inverse problem of CD-SAXS.

Acknowledgment

The authors would like to thank the technical support from the Experiment Center for Advanced Manufacturing and Technology, School of Mechanical Science and Engineering, HUST. They also would like to thank the technical support from the SAXS beamline of the Shanghai Synchrotron Radiation Facility (SSRF).

References

[1] T. Shohjoh et al., "Inspection and metrology challenges for 3 nm node devices and beyond," in *IEDM Tech. Dig.*, San Francisco, CA, USA, Dec. 2021, pp. 3.3.1–3.3.4.

[2] N. G. Orji et al., "Metrology for the next generation of semiconductor devices," *Nat. Electron.*, vol. 1, no. 10, pp. 532–547, 2018.

[3] W. Yang et al., "Line-profile and critical-dimension monitoring using a normal incidence optical CD metrology," *IEEE Trans. Semicond. Manuf.*, vol. 17, no. 4, pp. 564–572, Dec. 2004.

[4] J. Reche, P. Gergaud, Y. Blancquaert, M. Besacier, and G. Freychet, "Shape and roughness extraction of line gratings by small angle X-ray scattering: Statistics and simulations," *IEEE Trans. Semicond. Manuf.*, vol. 35, no. 3, pp. 425–431, Aug. 2022.

[5] W.-L. Wu et al., "Review of the key milestones in the development of critical dimension small angle X-ray scattering at national institute of standards and technology," *J. Micro/Nanopatterning, Mater., Metrol.*, vol. 22, no. 3, Apr. 2023, Art. no. 031206.

[6] R. Suenaga, Y. Ito, T. Goto, and K. Omote, "Precise 3D profile determination of high aspect ratio hole patterns by transmission small-angle X-ray scattering," *Jpn. J. Appl. Phys.*, vol. 62, no. 9, Sep. 2023, Art. no. 096502.

[7] T. Yang, X. Chen, J. Zhang, J. Ma, and S. Liu, "Form factor of any polyhedron and its singularities derived from a projection method," *J. Appl. Crystallogr.*, vol. 56, no. 1, pp. 167–177, Feb. 2023.

[8] D. F. Sunday, S. List, J. S. Chawla, and R. J. Kline, "Determining the shape and periodicity of nanostructures using small-angle X-ray scattering," *J. Appl. Crystallogr.*, vol. 48, no. 5, pp. 1355–1363, Oct. 2015.

[9] A. F. Hannon, D. F. Sunday, D. Windover, and R. Joseph Kline, "Advancing X-ray scattering metrology using inverse genetic algorithms," *J. Micro/Nanolithography, MEMS, MOEMS*, vol. 15, no. 3, Jul. 2016, Art. no. 034001.

[10] M.-A. Henn, H. Gross, F. Scholze, M. Wurm, C. Elster, and M. Bär, "A maximum likelihood approach to the inverse problem of scatterometry," *Opt. Exp.*, vol. 20, no. 12, p. 12771, Jun. 2012.

[11] H. Gross, M.-A. Henn, S. Heidenreich, A. Rathsfeld, and M. Bär, "Modeling of line roughness and its impact on the diffraction intensities and the reconstructed critical dimensions in scatterometry," *Appl. Opt.*, vol. 51, no. 30, p. 7384, Oct. 2012.

[12] B. R. Pauw, "Everything SAXS: Small-angle scattering pattern collection and correction," *J. Phys., Condens. Matter*, vol. 25, no. 38, Aug. 2013, Art. no. 383201.

[13] L. Kirkup and R. B. Frenkel, *An Introduction to Uncertainty in Measurement: Using the GUM (Guide to the Expression of Uncertainty in Measurement)*, 11st ed., New York, NY, USA: Cambridge Univ. Press, 2006.

[14] D. F. Sunday, S. List, J. S. Chawla, and R. Joseph Kline, "Evaluation of the effect of data quality on the profile uncertainty of critical dimension small angle X-ray scattering," *J. Micro/Nanolithography, MEMS, MOEMS*, vol. 15, no. 1, Jan. 2016, Art. no. 014001.

[15] D. F. Sunday et al., "Determination of the internal morphology of nanostructures patterned by directed self assembly," *ACS Nano*, vol. 8, no. 8, pp. 8426–8437, Aug. 2014.

[16] D. F. Sunday, E. M. Ashley, L. Wan, and R. J. Kline, "Template-polymer commensurability and directed self-assembly block copolymer lithography," *J. Polym. Sci. B, Polym. Phys.*, vol. 53, no. 8, pp. 595–603, Feb. 2015.
[17] D. F. Sunday et al., "X-ray characterization of contact holes for block copolymer lithography," *J. Appl. Crystallogr.*, vol. 52, no. 1, pp. 106–114, Feb. 2019.
[18] A. C. Davison and D. V. Hinkley, *Bootstrap Methods and Their Application*, 11st ed., New York, NY, USA: Cambridge Univ. Press, 1997.
[19] W. H. Press, S. A. Teukolsky, W. Y. Vetterling, and B. P. Flannery, "Modeling of data," in *Numerical Recipes: The Art of Scientific Computing*, 3rd ed., New York, NY, USA: Cambridge Univ. Press, ch. 15, sec. 6, 2007, pp. 809–810.
[20] R. Rosa, "The inverse problem of ellipsometry: A bootstrap approach," *Inverse Problems*, vol. 4, no. 3, pp. 887–900, Jan. 1999.
[21] M. Campoy-Quiles, M. I. Alonso, D. D. C. Bradley, and L. J. Richter, "Advanced ellipsometric characterization of conjugated polymer films," *Adv. Funct. Mater.*, vol. 24, no. 15, pp. 2116–2134, Apr. 2014.
[22] R. A. Synowicki, C. M. Herzinger, J. T. Hall, and A. Malingowski, "Optical constants of electroplated gold from spectroscopic ellipsometry," *Appl. Surf. Sci.*, vol. 421, pp. 824–830, Nov. 2017.
[23] X. Chen, H. Gu, J. Liu, C. Chen, and S. Liu, "Advanced Mueller matrix ellipsometry: Instrumentation and emerging applications," *Sci. China Technolog. Sci.*, vol. 65, no. 9, pp. 2007–2030, Aug. 2022.
[24] T. Yang, X. Chen, S. Liu, J. Zhang, and S. Liu, "Condition-number-based measurement configuration optimization for nanostructure reconstruction by optical scatterometry," *Meas. Sci. Technol.*, vol. 34, no. 12, Aug. 2023, Art. no. 125001.
[25] F. Tian et al., "Small angle X-ray scattering beamline at SSRF," *Nucl. Sci. Tech.*, vol. 26, no. 3, pp. 1–6, Jun. 2015.

Tianjuan Yang received the Ph.D. degree in mechanical engineering from the Huazhong University of Science and Technology (HUST), Wuhan, China, in 2024.

She is currently working with Skyverse Technology Company Ltd., Shenzhen, China. Her research interests are optical metrology and small-angle X-ray scattering metrology.

Xiuguo Chen received the Ph.D. degree in mechanical engineering from the Huazhong University of Science and Technology (HUST), Wuhan, China, in 2013.

He worked as a JSPS Fellow at Tohoku University, Sendai, Japan, from 2016 to 2018. He is currently a Professor with the School of Mechanical Science and Engineering at HUST. His research interests are optics and X-ray-based nanometrology and instrumentation for advanced semiconductor manufacturing.

Shuo Liu received the M.S. degree in mechanical engineering from the Huazhong University of Science and Technology, Wuhan, China, in 2022, where he is currently pursuing the Ph.D. degree.

His research interests are scatterometry and deep learning for nanoscale metrology.

Jiahao Zhang received the B.S. degree in mechanical engineering from the Huazhong University of Science and Technology, Wuhan, China, in 2020, where he is currently pursuing the Ph.D. degree.

His research interests are small-angle X-ray scattering and experimental analysis in IC metrology.

Shiyuan Liu received the Ph.D. degree in mechanical engineering from Huazhong University of Science and Technology (HUST), Wuhan, China, in 1998.

He worked as a Visiting Scholar at the University of Manchester, Manchester, U.K., from 2000 to 2001. He is currently a Professor with the School of Mechanical Science and Engineering at HUST. His research interests are computational imaging and computational lithography, micro/nano measurement technology and instrumentation, and optical metrology and defect inspection for integrated circuit manufacturing.